SAND Number: SAND2007-0775P

SANDIA NATIONAL LABORATORIES
HYDROGEN SAFETY, CODES & STANDARDS PROGRAM

QUARTERLY PROGRESS REPORT FOR OCTOBER -- DECEMBER 2006.

SANDIA RESEARCH AND DEVELOPMENT PROJECT
SUBMITTED BY: **CHRIS MOEN AND JAY KELLER**
TEAM: **BILL HOUF, JEFF LACHANCE, CHRIS SAN MARCHI, BOB SCHEFER, AND BRIAN SOMERDAY**

Quarter 1 FY 2007 AOP Milestones

The first quarter work was executed at a "continuing resolutions" rate similar to FY06 spending, so some tasks are proceeding at a slower rate than they would under full funding. With new spending guidance from the program office, we intend to ramp up to the full spend rate in Q2. A synopsis of Q1 milestones is given below with a detailed discussion in the body of this report.

1.1.1 Milestone: Conduct public comment sessions on the proposed risk approach for "Quantifying Commercial Refueling Risk Drivers and Consequences" task. A risk-informed approach for quantifying separation distances, identifying risk drivers, and identifying required preventive and mitigation features has been presented at several forums including the Tech Team, IEA, and NFPA. The task is on track to apply the methodology to an example facility. Available results will be shared in public presentations at the IEA Task 19 meeting in January 2007 and the NHA meeting in March 2007.

1.1.4 Milestone: Characterize concentration field non-circular leaks for "Small Scale Hydrogen Release" task. Completed data acquisition and partially completed data reduction and analysis. Task will be completed in second quarter of FY07.

1.1.4 Milestone: Verify slow leak model against leak data for "Small Scale Hydrogen Release" task. This task is on track. Model results will be shared in public papers and presentations at the NHA and SAE meetings in March-April 2007.

1.1.5 Milestone: Complete simple validation of CFD code for numerical experiments using a model problem for "Effective and Safe Barrier Wall Design for Risk Reduction" task. The task start date has moved to Q2 FY07 because of the project spending limit in Q1. We did hold a one-day technical meeting in Q1 with other researchers involved in jet modeling to discuss model validation challenges.

1.2.1 Milestone: Design and build a heat transfer validation experiment for "Develop Heat Transfer Correlations for 70 MPa Refueling" task. The plans for the fast-fill fueling study have changed relative to the FY07 AOP. Powertech Labs will execute fast-fill fueling tests for a consortium of OEMs and energy companies. Sandia will contribute funds to the test consortium and we will use test data to calibrate heat transfer correlations for a refueling model.

1.3.2 Milestone: Complete publications for testing of duplex stainless steel and 316 stainless steels for "Materials Testing: Hydrogen-Assisted Slow Crack Growth" task. The publication on duplex stainless steel entitled "Mechanical Properties of Super Duplex Stainless Steel 2507 After Gas Phase Thermal Precharging with Hydrogen" has been submitted to Metallurgical *Transactions A*. The publication on 316 stainless steel is being reworked to accommodate data collected during FY06 Q4.

Unintended Releases, Small Leak Scenarios

Predicting flammability envelopes for unignited leaks of various sizes is necessary to a better understanding of potential safety hazards related to unintended releases through small leaks. Measurements are performed to develop and validate engineering models.

Measurements of the hydrogen concentration field in the region of a leak were carried out during FY06 using the Rayleigh scattering apparatus described in a previous quarterly report. During the present quarter, reduction of this data was continued with the primary goal to obtain statistical data that can be used to validate engineering and CFD models for predicting hydrogen leak behavior. Shown in Figure 1 are radial profiles of the time-averaged H_2 mass fraction, Y_{H2}, at several axial distances from the leak exit. The results shown are for a 1.91-mm diameter round leak at a Reynolds number, Re, of 2,384 and Froude number, Fr, of 268. At this high Froude number the flow is largely momentum dominated, with the effects of buoyancy becoming important only at the farthest downstream locations that were measured. The profiles show the typical Gaussian profiles expected in this type of jet-like flow. The maximum H_2 concentration exists at the centerline and decreases moving radially outward as more air is mixed with the hydrogen issuing from the leak. The maximum centerline concentration decreases with downstream distance as additional[1] air is entrained into the H_2 jet.

These profiles have been replotted in terms of jet similarity variables in Figure 2a, where the mean mass fraction is normalized by the centerline value, Y_{CL}, and the radial distance is normalized by $(z-z_o)$, where z and z_o are the axial distance from the leak exit and the axial location of the virtual origin, respectively. It can be seen that the profiles collapse onto the same curve. The present results for hydrogen also show good agreement with a best fit to the experimental data of Richards and Pitts[1] for jet flows of methane, propane and helium, which is indicated by the solid line. Shown in Figure 2b are the corresponding radial profiles of the H_2 mass fraction fluctuations. Again the data collapse onto a single curve and show good agreement with the data of Richards and Pitts[1] for other gases.

Previous measurements of the H_2 concentration field were limited to a round leak geometry to facilitate comparisons with the substantial data available in the literature for other gases (methane, propane, etc.) in this geometry. However, in an actual unintended release scenario, the shape of the leak opening is likely to vary. For example, while a round hole might originate from a broken pipe, a narrow slot could be caused by a pipe crack and an annular ring could result from an o-ring failure. In the last quarter we obtained measurements to characterize the effect of

[1] Richards, C. D. and Pitts, W. M., "Global Density Effects on the Self-Preservation Behavior of Turbulent Free Jets", J. Fluid Mech. 254, pp. 417-435 (1993).

leak shape on the global hydrogen dispersion characteristics (length, width, expansion rate and the extent of the flammability envelope). The data is currently being reduced and will be used to extend the current engineering model to predict the effect of leak shape on jet flammability contours in small, slow leak scenarios.

Complementary velocity data sets were obtained at the same leak conditions at which the hydrogen concentration data were obtained to characterize the velocity field and provide additional model validation data. The measurements were obtained in a round jet geometry using Planar Imaging Velocimetry (PIV) at Froude numbers of 268, 152 and 99 to characterize the effect of buoyancy. These Froude numbers corresponds to Reynolds numbers of 2,384, 1,353 and 884. Shown in Figure 3a is the axial velocity component along the centerline, U_{cl}, as a function of axial distance. Figure 3b shows the inverse centerline velocity as a function of axial distance. At the highest Reynolds number of 2,384 (momentum-dominated regime), for z/d<100 the decay rate of U_{cl} follows a 1/z dependence, which is consistent with other momentum-dominated jets found in the literature. A best fit to the data in this momentum-dominated region is indicated by the solid line. However, for z/d >100 the present data departs from this line and falls increasingly below it as z/d increases, indicating a decrease in the axial velocity decay rate. Similar results are seen for the two lower Reynolds number cases, where U_{cl} follows a 1/z dependence at upstream locations and then increasingly departs from this behavior farther downstream. Also, the location where this departure first occurs moves upstream with lower Re, and thus higher Fr. Similar departure from momentum-dominated behavior was seen in the previously reduced H_2 mole fraction data (see below in Figure 4) and is attributed to the increasing influence of buoyancy.

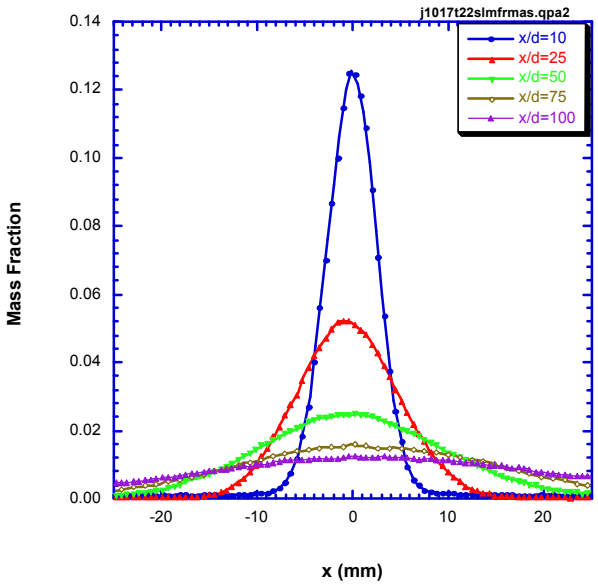

Figure 1 Radial profiles of H_2 mass fraction in turbulent, momentum-dominated flow regime. Leak diameter is 1.91 mm.

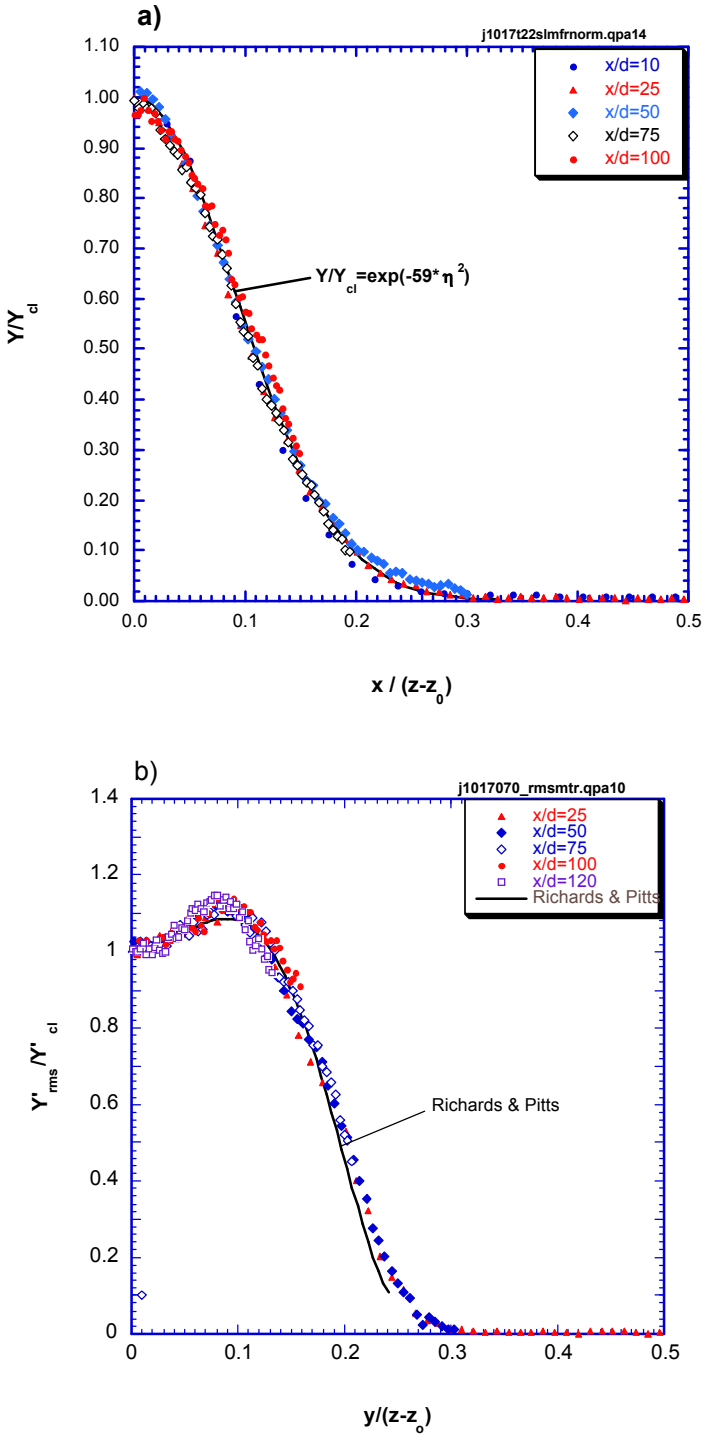

Figure 2 Normalized radial profiles of mean H_2 mass fraction and mass fraction fluctuations.

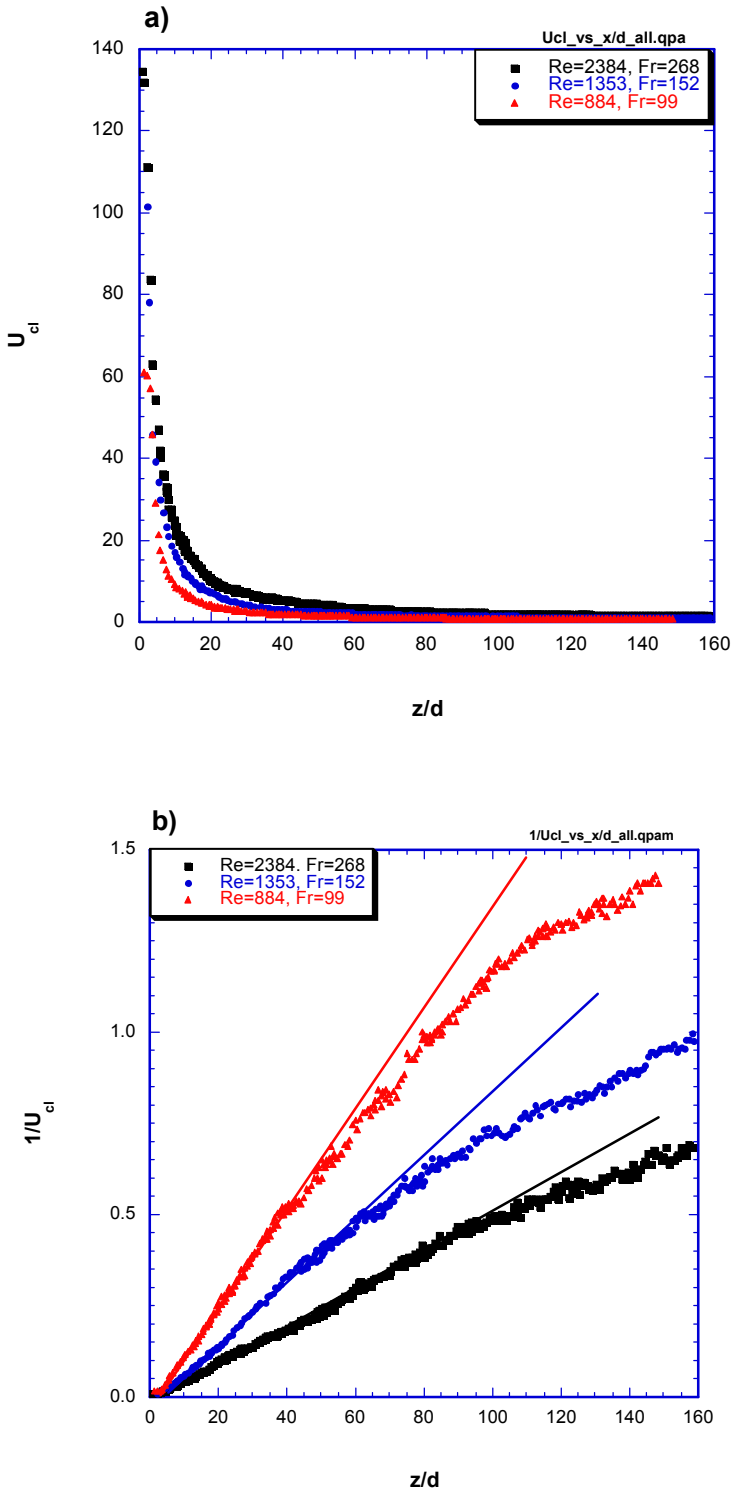

Figure 3 Centerline profiles of mean axial velocity and inverse mean axial velocity. Leak diameter is 1.91 mm.

During this quarter a new entrainment correlation was developed that extends the slow leak models range and allows it to better capture lower levels of concentration decay (down to approximately 4%) in situations where the jet becomes more locally buoyant. The model has been validated by comparison to vertical buoyant jet data from the Sandia slow leak experiment.

Previously, a jet entrainment correlation based on experimental data of Ricou and Spalding[2] was used in the model. The Ricou and Spalding entrainment law that is of the form

$$E = 0.282 M_o^{1/2} \rho_\infty^{-1/2} \tag{1}$$

where ρ_∞ is the density of the ambient air and M_o is the initial momentum of the jet ($M_o = \pi \rho_o D_o^2 u_o^2/4$). Simulations with the Ricou and Spalding entrainment function agreed with data from the Sandia slow leak experiment in the early development (lower *z/d*) region of the jet where the flow is momentum dominated, but failed to account for the increase in jet entrainment rate due to the increased importance of buoyancy relative to momentum as the jet entered the higher *z/d* region.

To incorporate this increase in entrainment due to buoyancy and improve the agreement with the Sandia slow leak experimental data an entrainment correlation of the form

$$E = E_{mom} + E_{buoy} \tag{2}$$

was postulated based on an approach similar to that presented by Hirst[3]. In this approach the turbulent entrainment rate is considered to be composed of a component due to momentum (E_{mom}) and a component due to buoyancy (E_{buoy}). In the current version of the slow leak model the component of entrainment due to jet momentum (E_{mom}) is calculated from the Ricou and Spalding law (Eq.(1)) as before

$$E_{mom} = 0.282 M_o^{1/2} \rho_\infty^{-1/2} \tag{3}$$

but now, in addition, a component due to buoyancy (E_{buoy}) is calculated from an expression of the form (Hirst[2])

$$E_{buoy} = \frac{a_2}{Fr_l} (2\pi U_{cl} b) \sin\theta \tag{4}$$

where U_{cl} is the jet centerline velocity, b is the radius of the jet boundary, θ is the angle between the jet centerline and the horizontal, a_2 is an empirically determined constant, and Fr_l is the local Froude number given by an expression of the form

---

[2]Ricou, F. P. and Spalding, D. B., "Measurement of Entrainment by Axisymmetric Turbulent Jets", J. Fluid Mech, 11, pp.21-31, 1961.

[3] E.A. Hirst, "Analysis of Buoyant Jets within the Zone of Flow Establishment," Oak Ridge National Laboratory, Report ORNL-TM-3470, 1971.

$$Fr_l = \frac{U_{cl}^2}{(gD(\rho_\infty - \rho_{cl})/\rho_{exit})} \tag{5}$$

In the local Froude number expression, U_{cl} is the local jet centerline velocity, g is the acceleration due to gravity, D is the leak diameter, ρ_∞ is the ambient density, ρ_{cl} is the local jet centerline density, and ρ_{exit} is the exit density of hydrogen. In the initial development of the jet, momentum dominates, the local Froude number (Fr_l) is high, and hence the $1/Fr_l$ dependence of Eq. (4) causes E_{buoy} to be negligibly small compared to E_{mom} in the total entrainment expression (Eq. (2)). As the jet progresses, buoyancy forces become more important, the local Froude number decreases, and the E_{buoy} term begins to contribute, producing the increase in the local jet entrainment observed in the Sandia slow leak experiments. The constant a_2 in Eq. (5) is typically empirically determined, and Hirst[2] reports a value of $a_2 = 0.97$. In this work the value of a_2 was determined to give the best agreement with the concentration decay data from the Sandia slow leak experiments for vertical hydrogen jets with exit densimetric Froude numbers (Fr_{den}) of 99, 152, and 268. For the $Fr_{den} = 268$ vertical jet data the value of $a_2 = 0.97$ reported in the literature by Hirst[2] yielded the best agreement with the data, hence a value of $a_2 = 0.97$ was used for all slow leak simulations with Fr_{den} equal to or greater than 268. The expression developed for a_2 is of the form

$$\begin{aligned} a_2 &= 17.313 - 0.11665 Fr_{den} + 2.0771 x 10^{-4} Fr_{den}^2 \qquad && Fr_{den} < 268 \\ a_2 &= 0.97 && Fr_{den} \geq 268 \end{aligned} \tag{6}$$

The entrainment rate for a buoyant jet can also be expressed in terms of the local jet centerline velocity, U_{cl}, and radius, b, in an expression of the form[4]

$$E = 2\pi b \alpha U_{cl} \tag{7}$$

where α is the entrainment constant. As buoyancy becomes more dominate in the jet, it has been experimentally observed that the value of the entrainment constant, α, in Eq. (7) approaches the limiting value of $\alpha = 0.082$ for a pure plume[5]. A comparison of simulations from the slow leak model using the entrainment law of Eq. (7) with concentration data from the Sandia slow leak experiments indicates that the Sandia data for vertical hydrogen jets also exhibits this limiting plume entrainment behavior ($\alpha = 0.082$) in the far-field. Hence, the plume limiting entrainment rate is also enforced in the current slow leak entrainment model by using Eq. (7) in conjunction with Eqs. (2), (3), (4) to compute how the value of α increases as the jet progresses from the momentum-dominated near-field to the more buoyantly dominated far-field.

$$\alpha = \frac{E}{2\pi b U_{cl}} \tag{8}$$

---

[4] B. Gebhart, D.S. Hilder, and M. Kelleher, "The Diffusion of Turbulent Buoyant Jets," Advances in Heat Transfer, Vol. 16, Academic Press, Inc., 1984.

[5] E.J. List and J. Imberer, "Turbulent Entrainment in Buoyant Jets and Plumes," Proc. Amer. Soc. Civ. Eng., J. Hydraulic Div., pp. 1461-1474, 1971.

When the value of α given by Eq. (8) reaches or exceeds the limiting plume value of $\alpha = 0.082$, then the entrainment function of Eq. (3) is replaced with the entrainment function given by Eq. (7) using the constant limiting value of $\alpha = 0.082$ for the remainder of the calculation. This approach limits the maximum rate of entrainment for the model to the experimentally observed maximum rate of entrainment for a buoyant plume.

Figure 4 shows comparisons of centerline concentration decay from simulations with the slow leak model using the new entrainment function as compared to data for vertical hydrogen jets from the Sandia slow leak experiment. Results from the simulation are in good agreement (agreement to within approximately 6.5%), with the data for both the momentum-dominated near-field and the more buoyantly dominated far-field over the full range of Froude numbers (Fr_{den} = 99, 152, 268). Figure 5 shows the corresponding hydrogen mole fraction concentration contours from the simulations.

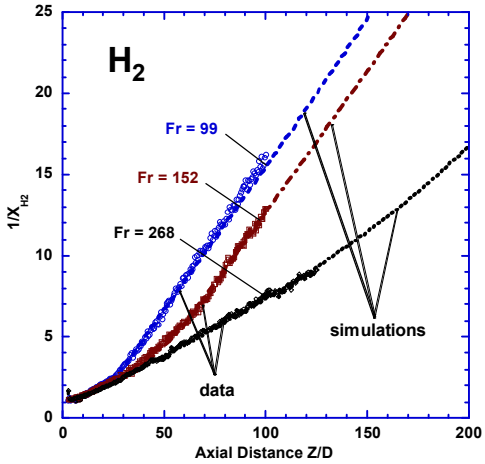

Figure 4 Comparison of simulations of the centerline concentration decay (X_{H2} = mole fraction) for vertical buoyant hydrogen jets with concentration data from the Sandia slow leak experiment (Fr_{den} = 99, 152, 269).

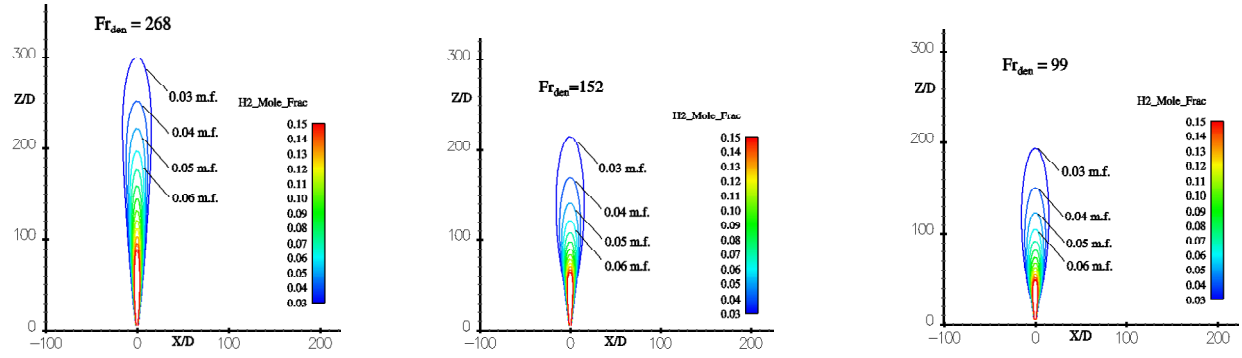

Figure 5 Hydrogen mole fraction concentration contours for simulations of vertical buoyant jets for conditions of the Sandia slow leak experiments (Fr_{den} = 99, 152, 269).

Hydrogen concentrations simulations from the slow leak model depend only on the exit densimeteric Froude number (Fr_{den}) and the initial angle of release (θ_0). A series of simulations were performed with the model for different exit densimetric Froude numbers (between 10 and 1000) and for initial jet angles starting at θ_0=0° (horizontal) and increasing in increments of 10° up to angle of θ_0=90° (vertical). Using this approach the concentration envelope for all possible leaks between θ_0=0° and θ_0=90° for a given exit densimetric Froude number can be computed. Figure 6 shows a plot of the concentration contour envelope for exit densimetric Froude numbers (Fr_{den}) of 10, 100, and 1000. Each point on the plot represents the annotated centerline concentration along the jet trajectory for calculations at one of the 10 angles between θ_0=0° and θ_0=90°. For Fr_{den} = 1000 the circular concentration profiles for hydrogen mole fractions of 4%, 6%, and 8% indicate that the leak concentration decay is dominated by the initial momentum of the jet and that buoyancy does not significantly influence the flow.

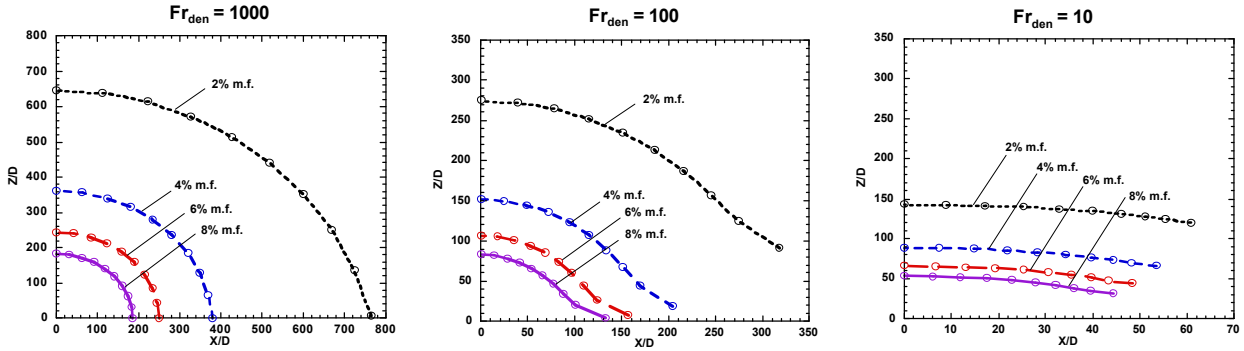

Figure 6 Centerline hydrogen mole fraction concentrations for different initial jet release angles (θ_0). Each point on a curve represents a slow leak simulation for an initial release angle between θ_0=0° (horizontal) and θ_0=90° (vertical) where the angle is changed in increments of 10°. The Z/D and X/D location of each point is the location on the jet centerline trajectory where that value of the concentration occurs.

The volumetric flowrate from a slow leak can be related to the exit densimetric Froude number and leak diameter. For a given diameter, leaks with a higher densimetric Froude number (Fr_{den}) have a higher exit velocity and are dominated more by initial momentum of the jet, while leaks with a lower densimetric Froude number have a slower exit velocity and are dominated more by buoyancy. Figure 7 shows a plot of hydrogen slow leak volumetric flowrate (Q) in standard liters per minute (slm) versus leak diameter (D) in millimeters for various exit densimetric Froude numbers (Fr_{den}).

The nondimensional radial distance (R/D) from the leak origin (X/D = 0.0, Z/D = 0.0) to each of the points on the concentration curves in Figure 6 can be compute from an expression of the form $R/D = ((X/D)^2+(Z/D)^2)^{1/2}$. Results of the calculations shown in Figure 6 can be used to compute the maximum radial distance, $(R/D)_{max}$, from the leak origin to the point where the jet concentration has decayed to a given concentration level. This maximum radial decay distance for all jet initial leak angles (between 0° (horizontal) and 90° (vertical)) is a parameter of importance to hydrogen safety codes and standards organizations. Table 1 shows values of the maximum radial distance $(R/D)_{max}$ from the leak origin to concentration decay levels of 2%, 4%, 6%, and 8% hydrogen mole fraction for exit densimetric Froude numbers of 10, 100, and 1000.

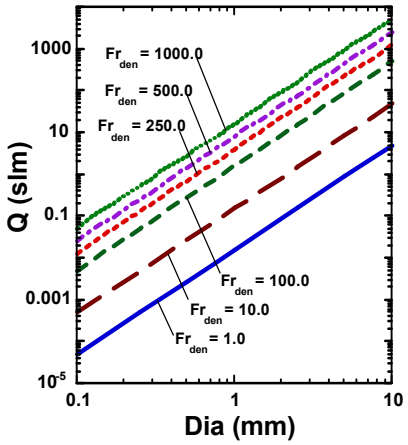

Figure 7 Hydrogen slow leak volumetric flow rate in standard liters per minute (slm) versus leak diameter for various leak exit densimetric Froude numbers (Fr_{den}).

Table 1 Maximum radial distance from leak origin to hydrogen mole fraction concentrations of 2%, 4%, 6%, and 8% for exit densimetric Froude numbers of 10, 100, and 1000.

Fr_{den}	$(R/D)_{max}$ 2%	$(R/D)_{max}$ 4%	$(R/D)_{max}$ 6%	$(R/D)_{max}$ 8%
10	142.92	88.86	66.25	54.37
100	331.22	205.14	156.79	132.57
1000	764.95	379.26	249.72	184.92

An invited paper entitled "Investigation of Small-Scale Unitended Releases of Hydrogen" by W.G. Houf and R. Schefer was written, reviewed, and accepted for presentation at the 2007 SAE World Congress to be held in Detroit, Michigan, April 16-19, 2007. The paper has also been recommended for publication in SAE Transactions Journal. An abstract for a paper entitled "Small-Scale Unintended Releases of Hydrogen" by W.G. Houf and R. Schefer was submitted and accepted for podium presentation for the 2007 NHA meeting to be held in San Antonio, Texas on March 19-22, 2007.

Marty Gresho, Bill Houf, and Jeff LaChance attended the NFPA 2 Hydrogen Technology Committee kickoff meeting held in Golden, Colorado on November 2-3, 2006. Gresho led the meeting as the committee chair. Houf presented a talk entitled Research and Development on Unintended Releases for Hydrogen Safety, Codes and Standards while LaChance gave a presentation on utilizing quantitative risk assessment (QRA) methods to establish risk-informed safety distances. During the month of November 2006 Houf was also appointed to the NFPA Vehicular Alternative Fuel Systems Committee.

We held a technical meeting on December 8, 2006, at the PG&E conference center in San Ramon, CA, to discuss model validation challenges for leak modeling using computational fluid dynamics. Participants included: Bill Houf, Greg Evan, Bob Schefer, Jay Keller, and Chris Moen from Sandia; Dennis Barley, Keith Gawlik, and Jim Ohi from NREL; Pierre Benard from

University of Quebec Hydrogen Research Institute; Andrei Tchouvelev from Tchouvelev and Associates; Bob Hay from TISEC. Discussions were focused around comparing Reynolds-averaged Navier-Stokes (RANS) calculations against experimental data and the engineering models. Discrepancies were identified for jets in ground effect. We identified some simple validation experiments we could perform at Sandia to help understand model results. We will continue to meet throughout the year and are working towards a joint paper for the International Hydrogen Safety Conference.

Unintended Releases, Barrier Wall Design

Jay Keller and William Houf participated in the HYPER Kickoff Meeting held at the Princess Hotel in Manchester England, on November 15 and 16, 2006. The following day (November 17) they traveled to nearby Chester England to hold discussions with Les Shirvill at Shell Global Solutions on hydrogen safety issues and explore possible areas for collaborations between Shell Global and Sandia in the area of hydrogen safety and combustion.

The HYPER Kickoff Meeting was a success and Sandia was recognized as a leader in the area of research for hydrogen safety and a key contributor and partner in the HYPER consortium. Sandia was also viewed as an important communication link between what is happening with the Hydrogen Codes and Standards Organizations in the United States and those in Europe. Sandia volunteered to take the leadership role in defining the statement of work for HYPER workpackages 4 and 5 which contain the bulk of the technical work for the project. We have written the draft statement of work for HYPER work packages 4 and 5 and it has been submitted to Dr. Stuart Hawksworth (HSE) the HYPER project Scientific Coordinator, and the work package 4 (Serge Chaudourne, CEA) and 5 (Thomas Jordan, FZK) leaders.

Technical work at Sandia begins in January 2007.

70 MPa Fast-Fill

The plans for the fast-fill fueling study have changed relative to the FY07 AOP. A consortium has formed to study 70 MPa fast-fill fueling requirements for the SAE J2601 standard, led by Powertech Labs. Powertech will perform the fast-fill tests. OEM partners are contributing in-kind fueling systems (i.e., the instrumented vehicular storage tanks). Other consortium members, including Sandia, are providing funds to execute the tests. As a consortium member, we participated in a bi-weekly teleconference in Q1 to plan the tests and define the consortium agreement. Sandia is still working (as of early January 2007) to place the contract for our contribution to the consortium. After Sandia gained approval for a contract agreement in Q1, the consortium decided to change the contractual language to solve funding problems for other consortium members. As a result, we have had to restart our contract approval process.

Once the contract is placed, we will have access to refueling trial technical data. We will use this data to calibrate heat transfer correlations to build a predictive model of the fast-fill process. We anticipate the modeling work will start in Q2.

Risk Analysis

Work this quarter continued on demonstrating a risk-informed approach for establishing safety (separation) distances for hydrogen refueling stations. The method established last quarter is currently being applied to a representative refueling facility. The focus of this work has been to further demonstrate the effect of key facility-specific parameters on risk-informed safety distances in addition to the parameters considered in the previous work (i.e., consequence measures and risk measures). The important facility parameters being evaluated include the hydrogen volume and pressure of the facility, the hydrogen generation method, and the availability and type of accident prevention and mitigation features. In addition, the current work is also demonstrating how parameter and modeling uncertainties can affect the safety distances.

Hydrogen refueling stations can vary in design but typically includes different onsite hydrogen generation methods, hydrogen gas compression, hydrogen storage, and vehicle dispensing areas. The associated risk and required safety distances can be influenced by the facility design. The efforts this quarter have been focused on estimating the required safety distances for an example facility design involving liquid hydrogen delivery and storage, and subsequent evaporation and pressurization for dispensing to vehicles. Efforts were made to construct an example facility design that complies with current codes and standards for hydrogen refueling facilities including National Fire Protection Association (NFPA) codes (e.g., NFPA 50A, 50B, 52, and 55), American National Standards Institute (e.g., ANSI/AIAAA G-095-2004), and the International Code Council (ICC) International Fire Code. Important code requirements incorporated into the example facility and subsequent analysis include:

- All equipment is assumed fabricated from materials suitable for hydrogen service and designed for the full range of pressures and temperatures to which they would be subjected. Electrical equipment is approved and appropriate for hydrogen facilities.
- Pressure vessels are equipped with pressure relief devices (e.g., safety valves and/or rupture discs) that vent at a safe location.
- Piping is not buried but can be place in trenches below ground with removal gratings. Liquid hydrogen piping is insulated to prevent personnel exposure to low temperatures and to prevent condensation of air. Combustible materials such as asphalt are not allowed under areas where air can be condensed as an explosive mixture could be created.
- Adequate filters are used to remove contaminants from the hydrogen system.
- Heat used to vaporize liquid hydrogen is applied indirectly using a transfer media such as air, steam, or water.
- The hydrogen system includes pressure regulators and pressure gauges at the outlet of each pump and compressor used in the facility. Temperature measurement is also provided at locations such as the output of a vaporizer to prevent liquid discharge.
- Control devices are installed to prevent system malfunctioning. For example, compressors are equipped with high discharge and low suction pressure automatic shutdown controls.

- Emergency shutdown valves are included at key locations in the system (e.g., at the output of the liquid hydrogen storage tank, at the inlet to a compressor, and at the vehicle dispenser) that shuts off the liquid and gas hydrogen supply during upset conditions including loss of power. Emergency shutdown can be automatically initiated (e.g., by gas or flame detectors) or initiated remotely by the facility operators. Emergency shutdown includes removal of electrical power form operating components such as pumps, compressors, and dispensers.
- Manual isolation valves are required at locations within the system including at the output of pressure containers and compressors and at the dispensers. Backflow check valves are also required at certain locations.
- Gas and flame detectors are installed such that gas and fire can be detected at any point along the facility equipment.
- A water spray system is available above hydrogen storage areas and over piping and pumps. The system can be manually or automatically actuated by the flame detector.
- Fueling nozzles are designed to prevent the escape of gas if the connector is not properly engaged or separates for some reason.
- The system is leak tested and equipment is subjected to periodic surveillance, calibration, and preventative maintenance. Operating procedures are in place to cover the full range of normal facility activities including refueling the liquid hydrogen storage tank.
- An emergency plan for the facility is required that includes emergency shutdown procedures that cover a wide range of anticipated emergencies. Personnel are trained to respond to emergencies

Quantitative risk assessment (QRA) models are currently being generated for the representative facility. The QRA includes identification of accident initiators; event trees that show the progression of an initiator to either mitigation or to some undesired consequence; fault tree models depicting how available mitigation systems can fail; data analysis to provide the accident frequency, human error probabilities, and component failure probabilities needed to quantify the QRA models; consequence assessment for each accident scenario; and quantification of the associated risk including an assessment of the uncertainty in the results. The QRA models cover a wide range of hydrogen releases including hydrogen releases from random component failures and human errors. The potential accidents, including hydrogen releases and other upset conditions, were identified by performing a Failure Modes Effects and Analysis (FMEA) of the example facility. The resulting accident initiators include both component failures and human errors, and result in both liquid and gaseous hydrogen releases.

Figure 8 illustrates a simplified accident event tree for evaluating the hydrogen release scenarios for each initiator. The event tree model and required data is adjusted as necessary to reflect the possible accidents in each of the facility components. As indicated, the accident sequence modeling represented by the event tree includes the potential for early accident mitigation through detection and isolation of the leak. Both automatic isolation and manual isolation are considered. The accident event tree also includes several phenomenological events that influence the accident sequence and resulting consequences. Included in these phenomenological events are the size of the leak, the potential for immediate ignition, the timing of delayed ignition, and the potential for propagation to other components. Fire suppression is included in the analysis as a means to prevent a leak scenario from escalating to other components. The

event tree also illustrates the resulting consequences for each sequence which includes jet fires of different magnitudes and durations, flash fires following delayed ignition of hydrogen, and the potential for hydrogen detonations. Although a continuous spectrum of leak sizes and durations, and possible consequences are possible, a discrete set of accident scenarios is reflected in the event tree model. The impact of the scenario binning will be evaluated as a sensitivity study.

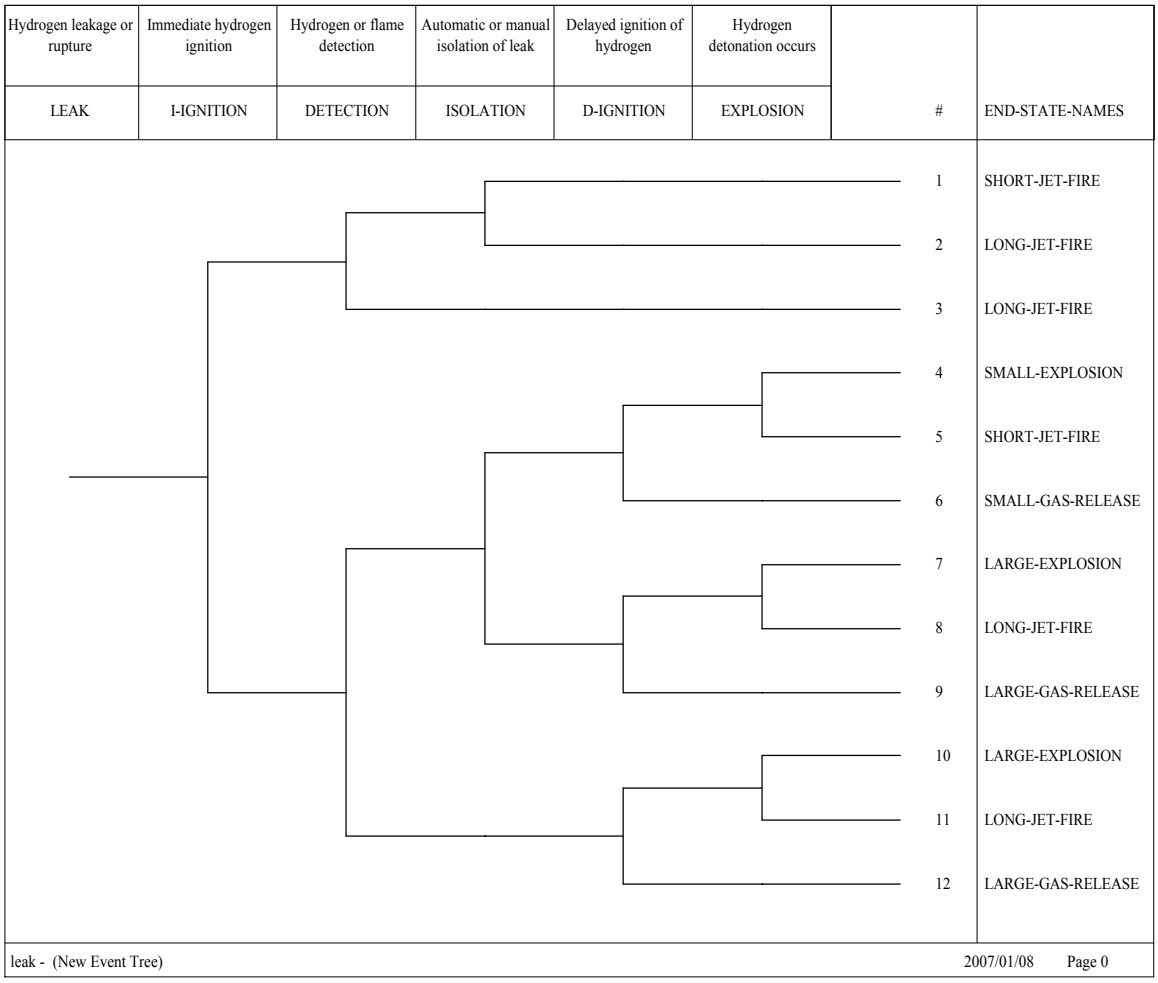

Figure 8 Hydrogen leakage/rupture event tree.

Supporting analyses are required to quantify the event tree shown in Figure 8. These analyses include construction of fault trees that depict how mitigation systems can fail. For the accident sequences shown in Figure 8, fault trees are required to determine how the hydrogen detection, system isolation valves, and fire suppression system can fail. In addition, failure data is required to quantify the accident scenarios. The data required includes component leakage frequencies, component failure rates (e.g., failure of a valve to close on demand), phenomenological event probabilities (e.g., hydrogen ignition probabilities), and human error probabilities (both as accident initiators and in responding to other initiators). Hydrogen-specific data is difficult to obtain and thus data from other sources was reviewed and representative values were selected. Example component leakage data, component failure data, and

phenomenological event data is shown in Table 2 through Table 4, respectively. The uncertainty distributions can be propagated through the QRA models to show the affect on the results. In addition, sensitivity studies can be performed for cases where there is substantial model uncertainty.

Table 2 Hydrogen component leakage frequencies.

Component	Mean Component Leakage Frequency [1]		
	Small Leak[2]	Large Leak[2]	Rupture[2]
Vessel	1E-3/yr	1E-4/yr	1E-5/yr
Pipe	5E-5/m-yr	5E-6/m-yr	5E-7/m-yr
Refueling Hose	0.1/yr	1E-2/yr	1E-3/yr
Pump	3E-3/yr	3E-4/yr	3E-5/yr
Compressor	3E-2/yr	3E-3/yr	3E-4/yr
Electrolyser	1E-4/yr	1E-5/yr	1E-6/yr
Vaporizer	1E-3/yr	3E-4/yr	5E-5/yr
Valve	1E-3/yr	1E-4/yr	1E-5/yr
Pipe Joints and Unions	3E-2/yr	4E-3/yr	5E-4/yr
Flange	3E-4/yr	3E-5/yr	NA
Filter	3E-3/yr	3E-4/yr	3E-5/yr
Instrument Line	1E-3/yr	3E-4/yr	5E-5/yr

Notes:

1. Leakage frequencies are generally assumed to be lognormally distributed (the exception is refueling hoses). The Error Factors (EF) for the distributions are assumed to be 10 for small and large leaks, and 30 for ruptures.
2. The size of the leak for a component can be related to either the pipe diameter or area (A). For example, a small leak = 0.01A, a large leak = 0.1A, and a rupture = A. A continuous or finer set of discrete leakage frequencies can be obtained by establishing a relationship between the leakage frequency and the leak diameter or area (e.g., the leakage frequency can be made a function of the inverse of the leak diameter).

The QRA analysis requires the evaluation of the consequences for each hydrogen release scenario. As indicated previously, these consequences can include different levels of radiative heat fluxes, flash fires (i.e., conflagrations), and potential hydrogen detonations. Sandia computer models are being used to predict the behavior of jet flames and hydrogen concentrations to determine the resulting consequences for some accident sequences. Additional models, required to evaluate the potential for hydrogen conflagrations and detonations and the resulting consequences, are being evaluated.

Table 3 Component failure data.

Component	Failure Mode	Mean Failure Rate[1]
Manual Valve	Fail to Open or Fail to Close	1E-4/demand (3)

Check Valve	Fail to Open	1E-4/d (3)
	Fail to Close	1E-3/d (3)
Motor-Operated Valve	Fail to Open or Fail to Close	3E-3/d (3)
	Spurious Operation	5E-7/hr (10)
Pressure Regulator Valve	Fails to Operate	2E-3/d (3)
Safety Relief Valve	Failure to Open for Pressure Relief	1E-5/d (3)
	Failure to Reclose	1E-2/d (3)
Compressor	Fail to Start	5E-3/d (5)
	Fail to Continue to Run	5E-5/hr (3)
Pump	Fail to Start	1E-3/d (10)
	Fail to Continue to Run	1E-4/hr (10)
Instrumentation	Failure to Operate	3E-6/hr (3)
Notes: 1. Failure rates are assumed to be lognormally distributed. The error factors for the distributions are shown in parenthesis.		

Finally, the current work is also demonstrating how to include parameter and modeling uncertainties in the methodology. To provide as complete a picture of the impact of uncertainty on the safety distances, parameter uncertainty is being propagated through the models. The resulting distributions can be used to identify different confidence levels in the resulting safety distances. In addition, sensitivity studies are being performed to evaluate the significance of the facility design on the safety distances. For the example facility currently being evaluated, potential sensitivities include whether the liquid hydrogen tank is below ground and whether hydrogen compressors are used instead of a liquid pump to raise the hydrogen pressure. Future efforts may include sensitivity studies on the impact of onsite hydrogen generation methods such as electrolysis and hydrocarbon reforming, and piped delivery of hydrogen gas on refueling station safety distances.

Table 4 Phenomenological event probabilities.

Event	**Mean Probability of Event**		
	Small leak	**Large Leak**	**Rupture**
Immediate hydrogen gas ignition	8E-3	5.3E-2	0.23
Delayed hydrogen gas ignition	4E-3	0.27	0.12
Explosion given delayed ignition	0.04	0.12	0.3
Liquid hydrogen ignition	0.01	0.03	0.08

Materials Compatibility

Chapters on duplex stainless steels and ferritic stainless steels were published on the Technical Reference for Hydrogen Compatibility of Materials website (www.ca.sandia.gov/matlsTechRef) in October 2006. Chapters on carbon steels and aluminum alloys are in preparation and are expected to be published in February 2007. Completion of chapters on carbon steels and aluminum alloys has been delayed due to significant activity in developing laboratory testing capabilities, namely the glove box and system for dynamic loading of materials in high-pressure hydrogen gas.

The glove box for preparing crack-growth specimens in a low-oxygen environment was successfully tested. The function of the glove box is to preclude the formation of oxides on the surfaces of crack-growth specimens after loads are applied, enabling hydrogen uptake into the specimens during subsequent exposure to hydrogen gas. This principle was tested by preparing a set of air-melted 4340 low-alloy steel specimens in the glove box then subsequently conducting crack-growth experiments in high-pressure hydrogen gas. The general procedures were as follows: 1) the crack-growth specimens and hydrogen gas pressure vessel were placed in the glove box containing argon gas with approximately 1 ppm oxygen, 2) the crack-growth specimens were bolt-loaded using a rotary actuator, 3) the crack-growth specimens were placed in the pressure vessel, which was then sealed using a lever arm attached to a piston, and 4) the sealed pressure vessel containing argon gas was removed from the glove box, the argon was evacuated, then the vessel was filled with high-pressure hydrogen gas. These procedures ensured that the specimens were not exposed to air from the time the specimens were bolt-loaded to the time the pressure vessel was filled with hydrogen gas. After filling the pressure vessel with hydrogen gas at 100 MPa, cracking initiated in the 4340 steel specimens in less than 24 hours.

The short initiation time for hydrogen-assisted cracking in 4340 specimens prepared in the glove box suggests that the postulated effect of air-formed oxides impeding hydrogen uptake has been eliminated by preparing the specimens in a low-oxygen environment. Previous tests on 4340 and SA 372 Grade J low-alloy steels exhibited prolonged initiation times for hydrogen-assisted cracking, and this behavior was attributed to oxides that formed while preparing the specimens in air. Tests on 4340 and SA 372 Grade J were ultimately terminated because of the prolonged initiation times. Since the successful function of the glove box indicates that past difficulties associated with testing low-alloy steels can be circumvented, the test matrix planned for SA 372 Grade J, DOT 3AAX, and DOT 3T low-alloy steels has been revived. Tests on these three steels are receiving high priority because ASME is interested in the results.

An initial set of tests was conducted on the SA 372 Grade J steel. Crack-growth specimens were prepared in the glove box following the procedures described above, then the specimens were exposed to 100 MPa hydrogen gas. Hydrogen-assisted cracking initiated in the specimens in less than 24 hours, further confirming that preparing specimens in a low-oxygen environment has circumvented complications associated with preparing specimens in air. The crack-growth thresholds measured for the SA 372 Grade J steel are plotted in Figure 9 along with literature data for similar pressure vessel steels in high-pressure hydrogen gas. The thresholds for SA 372 Grade J are about 95 MPa$\sqrt{m}$, which are significantly greater than values for the 4145 and 4147 steels at 100 MPa hydrogen gas pressure. The results for SA 372 Grade J are surprising, since

this steel is nominally the same as the 4145 and 4147 steels represented in Figure 9, i.e., all three materials are quenched and tempered Cr-Mo steels. The comparison between the SA 372 Grade J and 4147 steels in Figure 9 is particularly striking, since these steels have identical yield strengths. While the metallurgical origin of the dramatically higher crack-growth threshold for SA 372 Grade J has not been identified, the improved properties may reflect changes in steelmaking practices that have evolved over the last 30 years. The crack-growth thresholds measured for SA 372 Grade J in 100 MPa hydrogen gas represent the type of data that are required in Article KD-10 recently composed by the ASME Boiler and Pressure Vessel Project Team on Hydrogen Tanks.

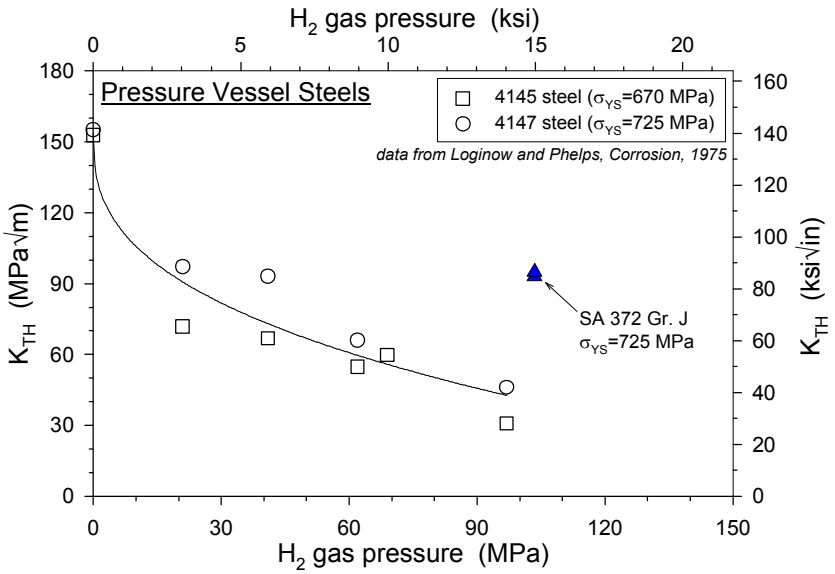

Figure 9 Crack-growth thresholds for SA 372 Grade J and two similar pressure vessel steels in high-pressure hydrogen gas.

An important milestone was reached in constructing the system for conducting materials tests under dynamic loading in high-pressure hydrogen gas. The MTS mechanical test frame was assembled and has been performing as expected. An image of the test frame is shown in Figure 10. The pressure vessel is being fabricated at Autoclave Engineers and when completed will fit in the load train of the mechanical test frame. The pressure vessel is expected to arrive at Sandia in February 2007. The test system will allow both fracture mechanics and tensile tests in hydrogen gas up to 140 MPa (20,000 psi) pressure.

Collaborations with a piping and valve component manufacturer have continued to be productive. Additional analysis of tensile deformation and fracture mechanics data from tests on hydrogen-charged and non-charged 316 stainless steels was conducted and a manuscript is in preparation to report the data. Tensile testing at subambient temperatures was initiated. The tensile flow curves of H-precharged materials, including type 316L stainless steel (Figure 11) as well as type 316 stainless steel and 22Cr-13Ni-5Mn stainless steel, are modestly affected by temperature. The ductility of H-precharged materials is nearly independent of temperature (Figure 12); any change in ductility may simply reflect temperature effects on the ductility of the non-charged materials (this testing is ongoing). Preliminary testing of notched-tensile specimens

also shows no significant effects of internal hydrogen on notched tensile strength, implying that the fracture properties are not strongly affected. Analysis on ductility of notched tensile specimens and fracture modes in the notched and smooth tensile specimens is in progress.

Figure 10 Mechanical test frame for dynamic loading of materials in high-pressure hydrogen gas.

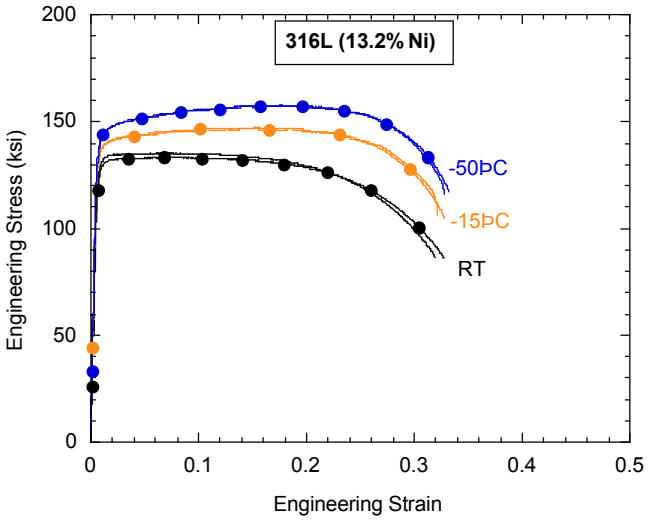

Figure 11 Tensile flow curves of a relatively high nickel type 316L stainless steel with internal hydrogen at several temperatures.

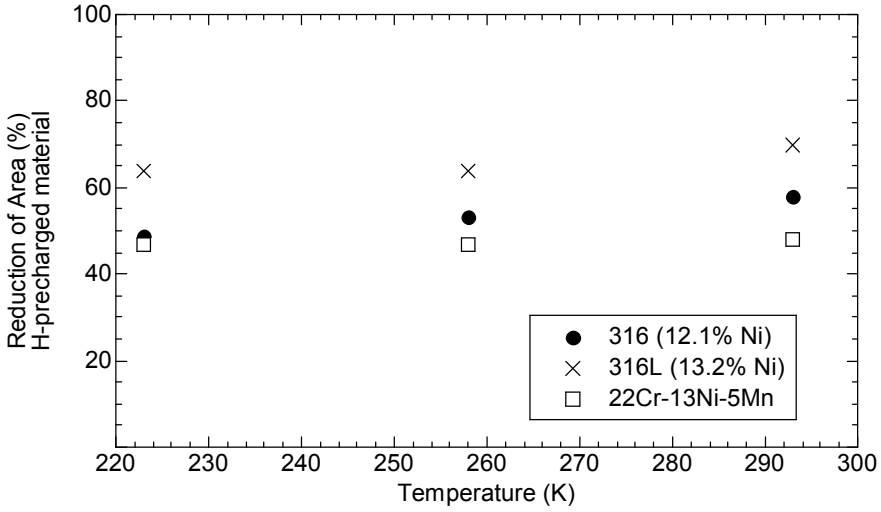

Figure 12 Ductility as measured by reduction of area as a function of temperature for three stainless steels in the H-precharged condition. All of these materials show good ductility.

Brian Somerday and Chris San Marchi participated in the quarterly meeting of the ASME Boiler and Pressure Vessel Project Team on Hydrogen Tanks.

A manuscript entitled "Effects of High-Pressure Gaseous Hydrogen on Structural Metals" was authored by Chris San Marchi and Brian Somerday and has been submitted to the conference proceedings of the SAE 2007 World Congress.

Codes and Standards Technical Team Participation

We have maintained active participation in the Codes and Standards Technical Team. This team tries to meet once per month with every other meeting being a face-to-face, and we participated in each of the monthly meetings during this last quarter. Detailed information on the team's activities can be found in the minutes from each meeting.